Surface Science 253 (1991) 116–128
North-Holland

The structure of thin NiO(100) films grown on Ni(100) as determined by low-energy-electron diffraction and scanning tunneling microscopy

M. Bäumer, D. Cappus, H. Kuhlenbeck, H.-J. Freund
Lehrstuhl für Physikalische Chemie I, Ruhr-Universität Bochum, Universitätsstrasse 150, 4630 Bochum 1, Germany

G. Wilhelmi, A. Brodde and H. Neddermeyer
Institut für Experimentalphysik, Ruhr-Universität Bochum, Universitätsstrasse 150, 4630 Bochum 1, Germany

Received 26 October 1990; accepted for publication 14 February 1991

A Ni(100) surface exposing terraces of approximately 100 Å width which are separated from each other by monatomic steps descending along the [010] direction has been oxidized above room temperature. Via intermediate formation of the well-known p(2 × 2) and c(2 × 2) chemisorbed phases, which are identified by LEED (low energy electron diffraction) and STM (scanning tunneling microscopy) in the present study, a thin film of 4–5 layers of NiO(100) builds up on the surface. The NiO layer consists of crystallites with a typical lateral extension of 50 Å as revealed by the STM data. SPA-LEED (LEED spot profile analysis) measurements allowed us to determine that the crystallite surfaces are tilted preferentially along the [011] and $[01\bar{1}]$ directions of the Ni(100) plane by an average angle of 8° with a half width of the angular distribution of 6°. We show that the development of the oxide islands most probably starts at the terrace edges of the metal surface. While the islands grow in size the strain between oxide and metal increases due to the large differences in the lattice constants of Ni and NiO. Part of the strain is compensated by a tilt of the islands induced via migration of Ni atoms from the step edges underneath the oxide islands. The generated NiO surface is characterized by two types of regions, namely the regions on the islands which are basically flat and contain regular NiO sites, covering 75–80% of the crystal surface, and the regions between the islands with many defect sites (20–25% of the surface area). The consequences of the structural properties of the NiO film on the adsorption of molecules, i.e., NO, are discussed in line with results of a previous study.

1. Introduction

The adsorption of oxygen on a Ni(100) surface has been investigated in numerous studies [1–26] starting with the one by MacRae in 1964 [1]. It is generally agreed that the adsorption of oxygen finally leads to the formation of nickel oxide. Its formation proceeds via several steps connected with two ordered chemisorption structures, namely a p(2 × 2) and a c(2 × 2) structure. In each structure the oxygen atoms reside in fourfold hollow sites [24]. A large number of detailed LEED studies of these structures may be found in the literature but atomically resolved STM measurements on O/Ni(100) have only be reported very recently [27].

Thiel and collaborators [25] have recently studied the temperature and exposure dependence of surface structures which form during oxidation of Ni(100) by quantitatively measuring electron diffraction spot intensities and profiles during adsorption of oxygen and annealing the surface up to above 500 K. They find a strong temperature dependence in the development of the LEED patterns of NiO. A hexagonal structure, interpreted as to be due to the formation of NiO(111) [16,22], is favored by adsorption temperatures below and close to 300 K whereas a (7 × 7)-like structure, first reported by Fadley and collaborators [21], is favored by adsorption temperatures of 300 to 400 K. If these layers are heated above 500 K the (7 × 7) and the NiO(111) structure "dispro-

0039-6028/91/$03.50 © 1991 – Elsevier Science Publishers B.V. (North-Holland)

portionate" into metallic Ni with chemisorbed oxygen and into NiO crystallites, i.e., a less and a more oxygen-rich phase [25].

One of the questions that was not answered in the important paper by Thiel and coworkers [25] is what is the role of surface defects in triggering the oxide formation and what is the size and the thickness of the oxide domains formed after oxidation at high temperatures.

In order to get some insight into these problems we have performed a combined high resolution LEED–STM study. We show that by starting from a Ni(100) surface exhibiting single-atom steps and terraces of about 100 Å width, p(2 × 2) and c(2 × 2) chemisorption phases are formed upon oxygen exposure. Our STM and LEED data indicate that steps on the surface are crucial to understand the oxidation mechanism. We show that already at low oxygen doses NiO crystallites preferentially start to grow at the step edges until finally the whole Ni(100) surface is covered with NiO islands. The islands are tilted with respect to the metallic substrate and we suggest that this is a consequence of the lattice misfit between metallic Ni and NiO.

We have used oxide films of similar structure as substrates to study molecular adsorption on oxide surfaces because such films allow the standard electron spectroscopic methods to be applied [26]. As an important result of the present study with respect to the adsorption investigations, published in a separate paper [26], we find that the region of the surface exposed to vacuum which is heavily defect-covered amounts to 20–25% of the total surface. It is not possible in the present study to specify in more detail the nature of the NiO defects but it is worthwhile to note that NO and CO adsorption does not take place to a noticeable amount onto these defects [26].

2. Experimental

The experiments have been performed in two different UHV chambers using different Ni(100) samples with similar misorientations, i.e, the descending step direction was approximately [010] in both cases (for the notation of directions used now and in the following, see fig. 1). All crystals were oriented within an accuracy of 1° using standard Laue technique. The UHV-systems were both equipped with conventional LEED systems, AES (Auger electron spectroscopy) and a quadrupole mass spectrometer for residual gas analysis. The chamber used for the SPA-LEED investigations additionally contained facilities for angular resolved UPS (ultraviolet photoelectron spectroscopy) and EELS (electron energy loss spectroscopy) and a SPA-LEED system of the type SPA-LEED-11 (Leybold AG) with a specified transfer width of more than 800 Å.

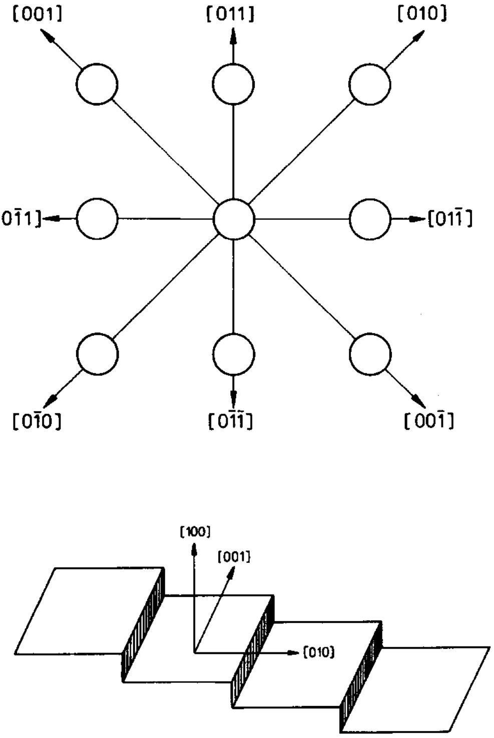

Fig. 1. Schematic plot showing the notation of directions on the Ni(100) surface used in this paper and the direction of the steps.

The Ni(100) sample used for the SPA-LEED studies was spot-welded to two tungsten rods which were connected to a liquid nitrogen reservoir such that the sample could be cooled below 100 K. Heating was possible by radiation from a filament mounted behind the crystal or by electron bombardment onto the reverse side of the crystal. The surface was prepared by repeated cycles of sputtering with He ions and heating to 800 K. Residual carbon was then removed by flashing the crystal in an oxygen atmosphere of 10^{-7} mbar followed by heating the crystal to 700 K for several minutes in 10^{-7} mbar hydrogen until LEED and AES indicated a clean and well-ordered surface. For the SPA-LEED investigations the NiO(100) film was prepared by repeated cycles of dosing 1200 L O_2 (1 L $= 10^{-6}$ Torr s) at $T = 570$ K and subsequent annealing to $T = 650$ K up to an oxygen dose of about 10000 L. After this treatment the LEED pattern exhibited broad NiO(100) spots. The Ni(100) substrate spots were strongly attenuated and additionally weak c(2 × 2) reflexes were visible.

Since details of the instrumentation used for the present STM measurements have been described elsewhere [28] only the main experimental conditions of the STM experiment are reported here. After mechanical and chemical polishing the Ni(100) substrates used for STM were cleaned in situ by cycles of argon ion bombardment (500 eV and 10 $\mu A/cm^2$ for a total time of typically 10 h) and annealing up to 1100 K until AES did not show contaminations of C, S and O within the limits of statistical accuracy. We estimate the sensitivity of the AES equipment to be in the order of 1% of a monolayer. A final contamination of the Ni(100) surfaces used for STM on the order of 1 to 3% of a monolayer cannot be ruled out. We note that extensive argon ion bombardment did not lead to a further reduction of the residual contamination (as concluded from the STM measurements) but rather to a roughening of the surface, which could only be removed by mechanical and chemical polishing and restarting the in situ surface treatment. The final substrate surfaces showed a clear LEED pattern of nonreconstructed Ni(100). Oxygen adsorption up to an exposure of 5000 L has been performed at room and elevated temperatures (up to 540 K) in the sample heating stage of the UHV system. Details of the experimental conditions of oxygen adsorption are mentioned in the figure captions. In agreement with previous findings [29] a p(2 × 2) LEED pattern was obtained for small exposures up to 2 L and preferentially on a slightly heated sample surface. With further exposure the c(2 × 2) pattern developed in LEED. For the highest exposure used in the STM measurements (5000 L) the c(2 × 2) pattern was still visible, in addition to the broad NiO-related beams. The pattern of the NiO-related beams was slightly tilted against the surface normal towards the $[01\bar{1}]$ direction very similar as was observed for the crystal used in the SPA-LEED investigations. The STM measurements turned out to be rather difficult mostly due to oxygen-induced changes of the tunneling tip leading often to a loss of atomic resolution. The atomic structure of "clean" Ni(100) could be resolved under optimum conditions of the STM and showed an atomic corrugation of less than 0.1 Å due to the Ni metal lattice. However, the high-voltage amplifier for the z-piezoelectric drive produced a noise equivalent to a few 0.01 Å in the data, which already limited the quality of the images. We have also tried to use STM in its spectroscopical mode [30] but due to the above-mentioned difficulties with the tip we were not able to stabilize the tunneling conditions under varying sample–tip bias voltages.

3. Results and discussion

The clean Ni(100) surface was characterized by energy dependent LEED spot profiles as shown in fig. 2. Intensity distributions of the zero-order beam along the [010] direction have been taken for electron energies between 50 and 190 eV. The energy dependence of the plotted intensity distribution is typical for a surface with a regular monotonic array of steps [31–35]. The splitting of the LEED spot amounts to approximately 2.5% of the surface Brillouin zone and indicates that the terrace width is close to 100 Å which is near to the value expected on the basis of a 1° misorientation of the crystal surface. From the energy dependence we deduce a step height of 1.76 Å, i.e., monatomic steps along the [010] direction. For comparison we show in fig. 3 a scanning tunneling micrograph of a similarly prepared Ni(100) surface. The individual terraces are clearly revealed, and the terrace widths and step orientation obtained on this part of the surface essentially agree with the findings from our kinematic LEED

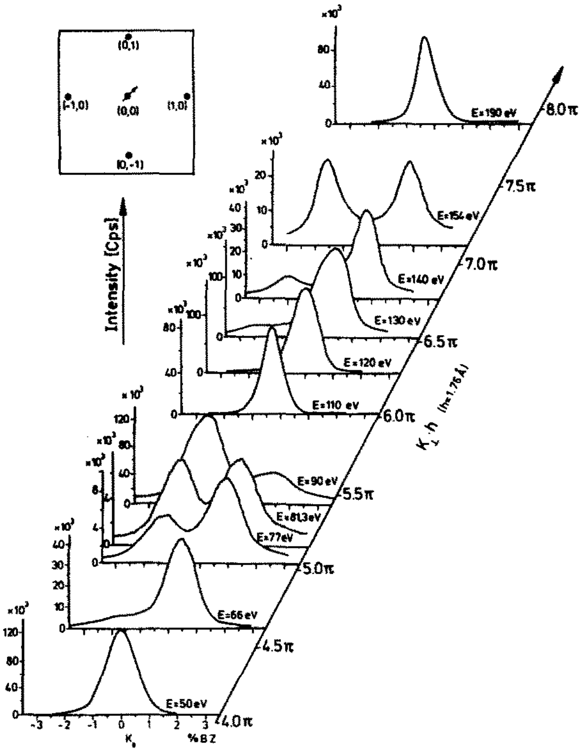

Fig. 2. LEED intensity profiles of the Ni-(0,0) beam of clean Ni(100) taken along the [010] direction for different electron energies.

analysis for the crystal used for the SPA-LEED studies. Note that the STM measurements show variations of both terrace width and step orientation on the various parts of the Ni(100) surface. In fig. 4 an atomically resolved STM image from a large Ni(100) terrace is reproduced. The corrugation due to the Ni(100) lattice of less than 0.1 Å in this case is clearly resolved. The influence of the noise in the z-value is visible in the form of a streaking parallel to the x-direction, which also corresponds to the direction of the individual scans of the surface. Note that a rather high tunneling current of 20 nA and a very small sample bias voltage of 1 mV have been employed for these measurements leading to a particularly small sample–tip separation. The presence of residual contamination on this surface may be deduced from the occurrence of dark local atomic features in bridge and 4-fold hollow sites. We have observed these local depressions on each atomically resolved measurement of Ni(100), they may even be recognized on the overview STM image shown in fig. 3. By counting the number of these local defect sites in fig. 4 we arrive at a concentration of 3% of a monolayer which is consistent with the possible presence of C, O, and S atoms on the surface in these limits.

The LEED analysis also shows that the Ni(100) crystal investigated with the SPA-LEED system is characterized by a pronounced mosaic structure [36]. This is revealed by the appearance of extra, weak spots even for in-phase scattering conditions where steps do not induce spot splittings [37–40]. We believe that the relatively large widths of the LEED spots of 0.8–1.0% of the surface Brillouin zone are due to mosaic structure. The resolution of the LEED instrument is better by a factor of three than the upper value [41].

If such a surface is exposed to increasing amounts of oxygen a p(2 × 2) and consecutively a c(2 × 2) pattern appear on the LEED screen. While the intensities of the c(2 × 2) spots have not yet reached their maximum value, oxide reflexes already start to grow in. As has been alluded to in the introduction there are several different oxides formed on the Ni(100) surface. Out of the three oxides described in the literature, i.e., the "hexagonal" NiO(111) [16,22], an oxide with a (7 × 7) pattern [21], and the NiO(100) [20] the latter is the most stable one, and we concentrate in the present study on its discussion.

Even before the growth of any of the oxide structures may be observed via LEED, STM reveals as well as EELS [42] the beginning of oxide nucleation. Fig. 5 shows an overview STM image from Ni(100) which has been exposed at room temperature to 10 L of oxygen. The characteristic terrace structure (similar to that shown in fig. 3) is still visible. However, the entire surface is randomly covered with additional protrusions (they appear in the image as bright spots), whose size varies between 10 and 50 Å. We ascribe these protrusions to NiO clusters, which grow on top of the ordered oxygen adlayer. Note that in LEED a clear c(2 × 2) pattern was still visible. It appears that at the step edges the *largest* NiO clusters present on the entire surface have been formed (see, e.g., locations denoted by A). We therefore

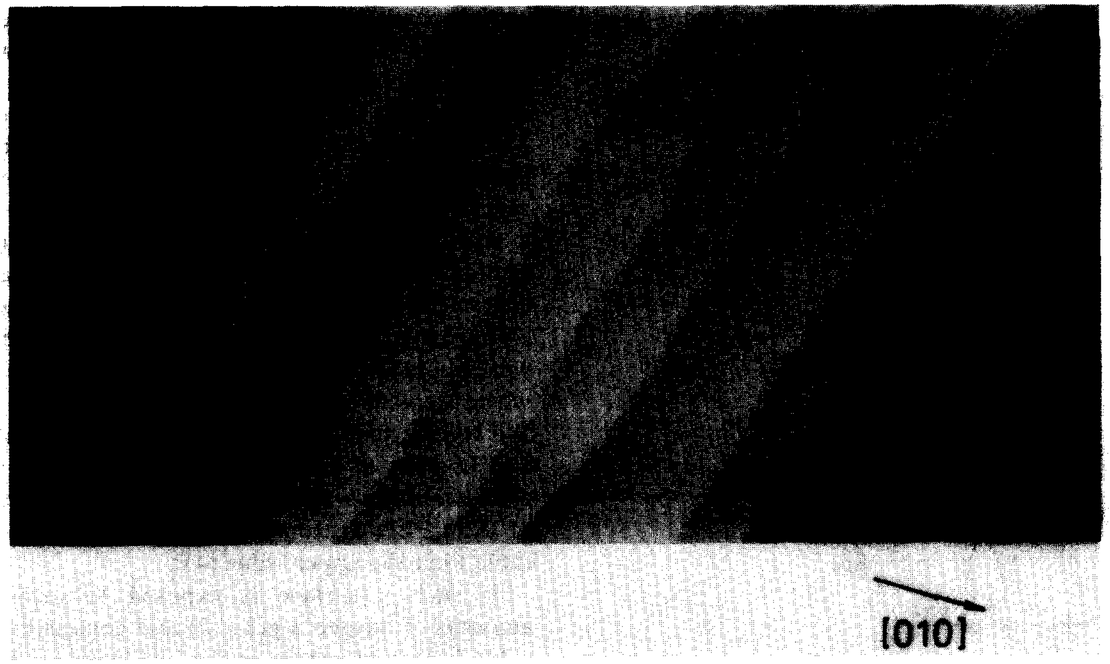

Fig. 3. Constant current topography (CCT) of Ni(100) showing monatomic steps with an area of 700 × 1400 Å^2 obtained at a sample bias voltage $U = 1$ V and a tunneling current $I = 1$ nA.

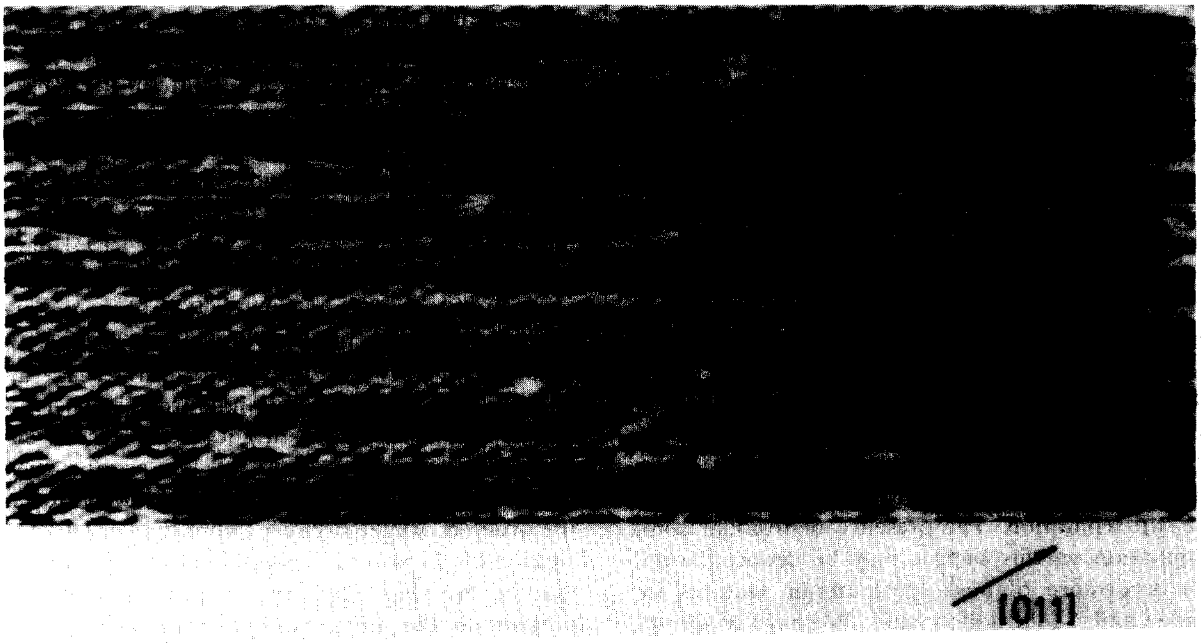

Fig. 4. CCT of Ni(100) obtained at $U = 1$ mV and $I = 20$ nA. The size is approximately 90 × 200 Å^2.

conclude that the step edges constitute *preferential* sites for growth of the NiO islands. It should be emphasized that in the LEED measurements the periodic splitting of the Ni substrate spots due to the existence of the regular array of terraces vanished during oxidation, which further supports the preferential growth of NiO at the step edges. An atomically resolved STM measurement of such a surface is reproduced in fig. 6. A monatomic step is running from the top to the bottom in the center of the figure. A large number of p(2 × 2) unit cells due to the adsorbed O atoms is clearly recognized (see, e.g., at A). In addition, smaller (e.g., at B) and larger (at C) additional protrusions are seen on the surface, which correspond to the random bright structures on fig. 5 and are explained by NiO clusters and islands. It has to be mentioned that on a hot Ni(100) surface (typically 470 K) the same oxygen exposure (10 L) does not lead to the growth of NiO clusters but rather to an ordered array of c(2 × 2) cells (not shown here). We also note that for a small exposure (2 L) on a hot substrate the STM images do not indicate the presence of NiO clusters but rather exhibit an ordered p(2 × 2) structure (not shown here). This means that in the initial stage of oxide growth and for small exposures NiO clusters are only found for room temperature adsorption. The density of these clusters on the terraces seems to be comparable to that of the defect sites on the cleaned substrate (fig. 4). Whether these defects initiate formation of NiO cluster cannot be concluded with certainty.

Repeated cycles of oxidation finally lead to the formation of a thick NiO layer with a (100) LEED pattern and absent or weak substrate spots [26].

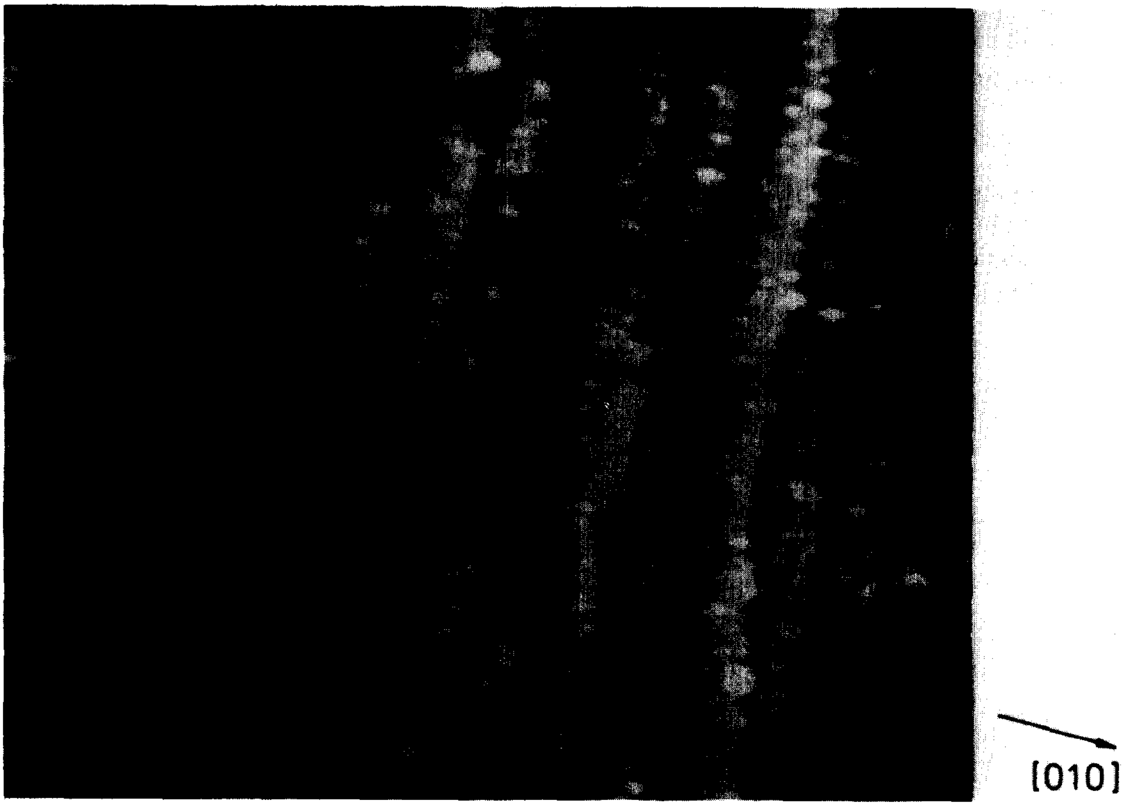

Fig. 5. CCT of Ni(100) exposed at room temperature to 10 L of oxygen (at a pressure of 10^{-7} mbar) and obtained at $U = 1$ V and $I = 0.5$ nA. The size is 800 × 1000 Å^2.

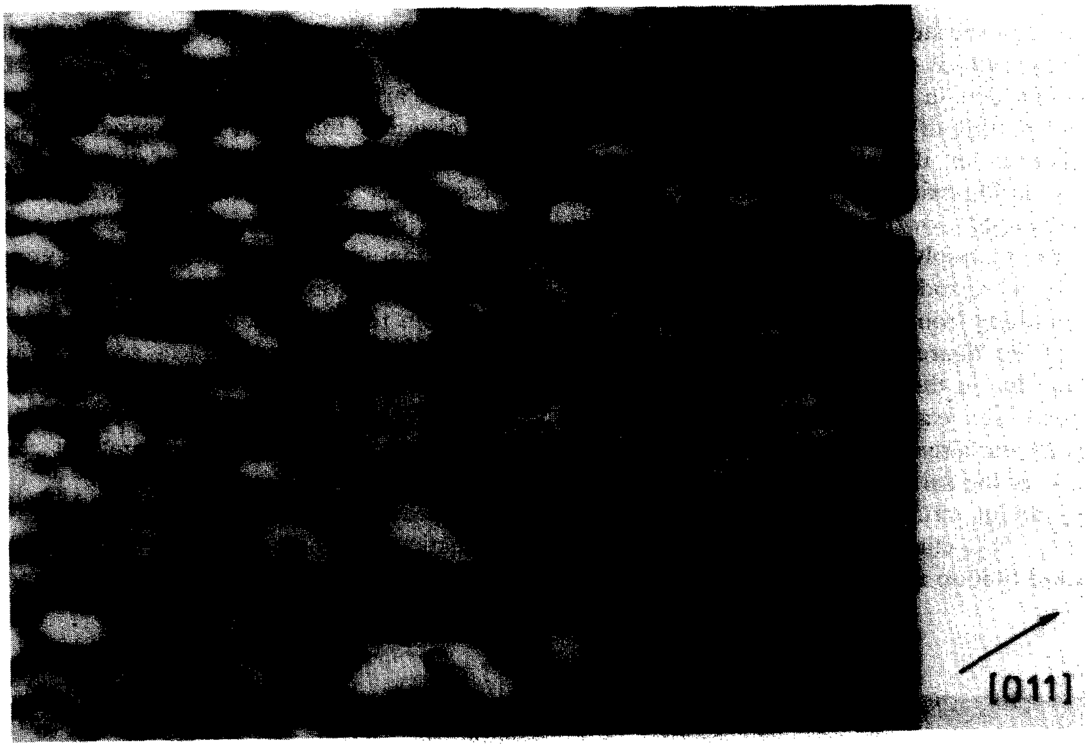

Fig. 6. CCT of Ni(100) exposed at room temperature to 10 L of oxygen (at a pressure of 10^{-7} mbar) and obtained at $U = -0.3$ V and $I = 0.5$ nA. The size is approximately 110 × 140 Å^2.

These LEED patterns of thin NiO films are well known in the literature and have been described on several occasions [15,16,22,26]. The observed spots are rather diffuse due to the pronounced misfit of the lattice constants of metallic Ni and NiO [43], i.e., the NiO lattice constant is by 16% larger than the Ni lattice constant. Consequently, the NiO spots form a smaller brillouin zone than

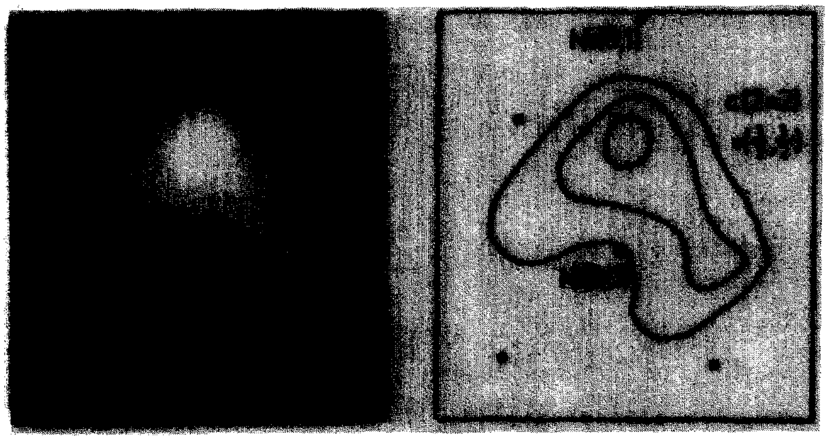

Fig. 7. LEED pattern of thin film NiO(100) taken with a SPA-LEED instrument at an electron energy of 70 eV. The sharp spots are due to the underlying Ni(100) substrate with a c(2 × 2)O superstructure.

the Ni spots, and they are usually symmetrically surrounded by the substrate spots. In contrast to the situation encountered in the literature the NiO spots in the present study are shifted mainly along two different [011]-like directions as shown in fig. 7. More precisely, the NiO spot intensity of the zero order beam is semicircularly distributed around the Ni-(0,0) beam, exhibiting maxima in the [011] and $[01\bar{1}]$ directions. A similar situation is encountered for beams of higher order. The cause for the observed NiO intensity distribution may be found by evaluating its dependence on the electron beam energy. We have studied the energy dependence in the range between 40 and 300 eV and found that there were only some energy ranges where the NiO spot exhibited count rates above 500 cps. Table 1 collects some experimental results of the SPA-LEED investigations. In the first columns the shifts of some NiO spot profile maxima with respect to the Ni-(0,0) beam and the halfwidths in fractions of the Ni(100) reciprocal lattice vector parallel to the surface for some beam energies are shown. As can be seen from the table the latter values are not constant but increase with increasing beam energy. This behaviour is consistent with NiO crystallites that are tilted with respect to the Ni(100) surface normal. The tilt angle has been calculated for each row of table 1 and is shown in the last column of this table. Within the statistics of the data these values do not vary with the beam energy as expected for tilted NiO crystallites. So we arrive at the picture as schematically shown in fig. 8: The oxide consists of crystallites which are tilted with respect to the substrate plane. Since the intensity distribution of the NiO(100)-(0,0) beam shows pronounced maxima along the [011] and $[01\bar{1}]$ directions (fig. 7) we conclude that the crystallites are

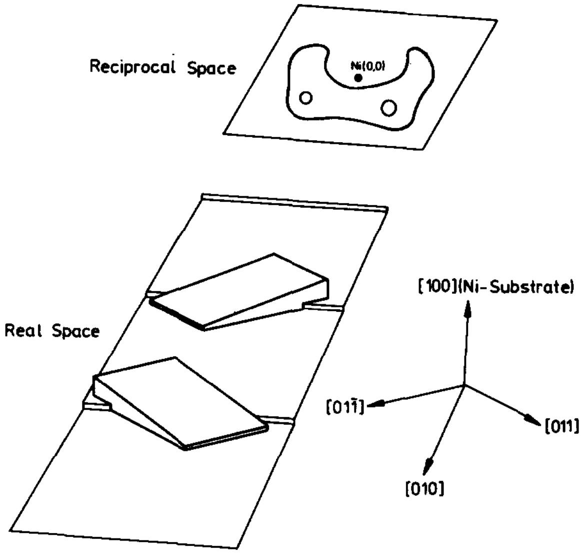

Fig. 8. Schematic plot showing two NiO crystallites on the step edges the substrate. The plotted crystallites are tilted along the two main tilting directions as observed by SPA-LEED and STM, i.e., [011] and $[01\bar{1}]$.

Table 1
Shift of some NiO reflexes and halfwidths for some electron energies given in percent of the [011] reciprocal lattice vector of the Ni(100) surface Brillouin zone; for $E = 200$ eV the Ni-(0,0) beam was not visible and so the shift of the NiO-(0,0) reflex could not be determined

E (eV)	Reflex	Shift (%BZ)	FWHM (%BZ)	Direction of the scan	Tilting angle (deg)
65	(0,0)	46	38	[011]	8.1
70	(0,0)	49	40	[011]	8.4
75	(0,0)	49	38	[011]	8.1
110	(0,0)	57	47	[011]	7.7
120	(0,0)	61	53	[011]	7.9
130	(0,0)	64	55	[011]	7.9
200	(0,0)	–	65	[011]	–
45	(1,0)	117	28	$[01\bar{1}]$	7.5
50	(1,0)	123	29	$[01\bar{1}]$	8.2
85	(2,0)	218	38	$[01\bar{1}]$	8.3

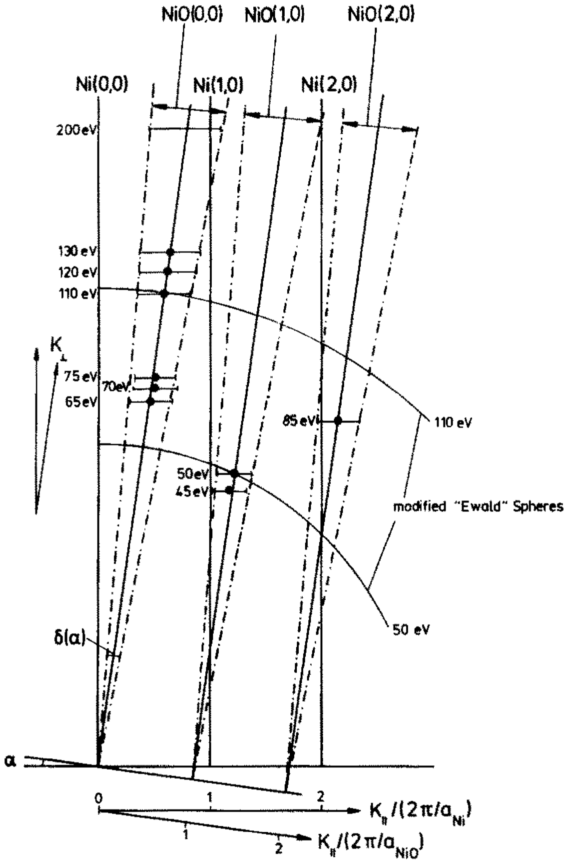

Fig. 9. Schematic plot showing the effect of the tilt of the NiO crystallites and the tilting angle distribution on the LEED reflexes in reciprocal space. The experimental values have been taken from table 1.

preferentially tilted along these directions. The relatively large halfwidths of the spot profiles are indicative of a rather wide spread of tilting angles. A quantitative evaluation of the data allows us to construct the reciprocal space as shown in fig. 9: The component of k perpendicular to the substrate as varied via the electron beam energy is plotted versus the component of k parallel to the substrate. The sections of circles shown in this figure are parts of modified Ewald circles [41] and represent lines of constant energy. Directly from this figure one may read off the most frequent tilt angle, i.e., $\alpha = 8.1° \pm 0.5°$ and the FWHM of the tilt angle distribution, i.e., $\delta(\alpha) = 6.6° \pm 0.8°$. If we remember that the descending step direction was [010] it is realized that there is no tilt of the oxide crystallites along ascending step directions of the substrate (see fig. 8). But there is a preferred tilting along [011] and [01$\bar{1}$] which are directions with descending steps indicating a relation between substrate steps and oxide crystallite tilt.

The picture deduced from the LEED investigations is qualitatively confirmed by the STM measurements for the oxide surface. Fig. 10 shows a STM picture of a surface which exhibits a similar LEED pattern as discussed above but has been prepared in the STM system. The LEED pattern of this particular sample showed a tilt of NiO crystallites towards the [01$\bar{1}$] direction of the same order as obtained on the sample used for the measurements depicted in fig. 7. We note that the corrugation of the reproduced surface area is on the order of 50 Å, which explains the lack of any visible step structures in fig. 10. Although the surface appears to be rather rough the ordering of the NiO islands is clearly visible as may be deduced from their general orientation along the [011] and in particular the [01$\bar{1}$] direction. On some of the NiO islands even a regular weak atomic corrugation is seen (which may not be apparent on the reproduction but is identified on the computer screen) although not sufficiently clear to derive more exact information on the atomic structure.

In order to investigate the development of the NiO spots as a function of oxygen exposure and its concommitant shift we present in fig. 11 a series of LEED traces along the [011] direction as a function of oxygen dose. In fig. 12 the dependence of the most frequent tilting angle, α, and the angular distribution, $\delta(\alpha)$, on oxygen exposure is plotted. There are several important observations: (i) the oxide spot intensity grows as the substrate spots intensity is attenuated, (ii) the oxide spot intensity maximum shifts as a function of dose, i.e., the separation from the substrate spot increases, (iii) the halfwidth of the oxide spot rapidly increases with increasing oxygen dose, then decreases slightly and levels off at a value slightly smaller than the maximum value.

As the next step, it is tempting to try to formulate a mechanism for the formation of the mosaic structure of the oxide film. Such a formu-

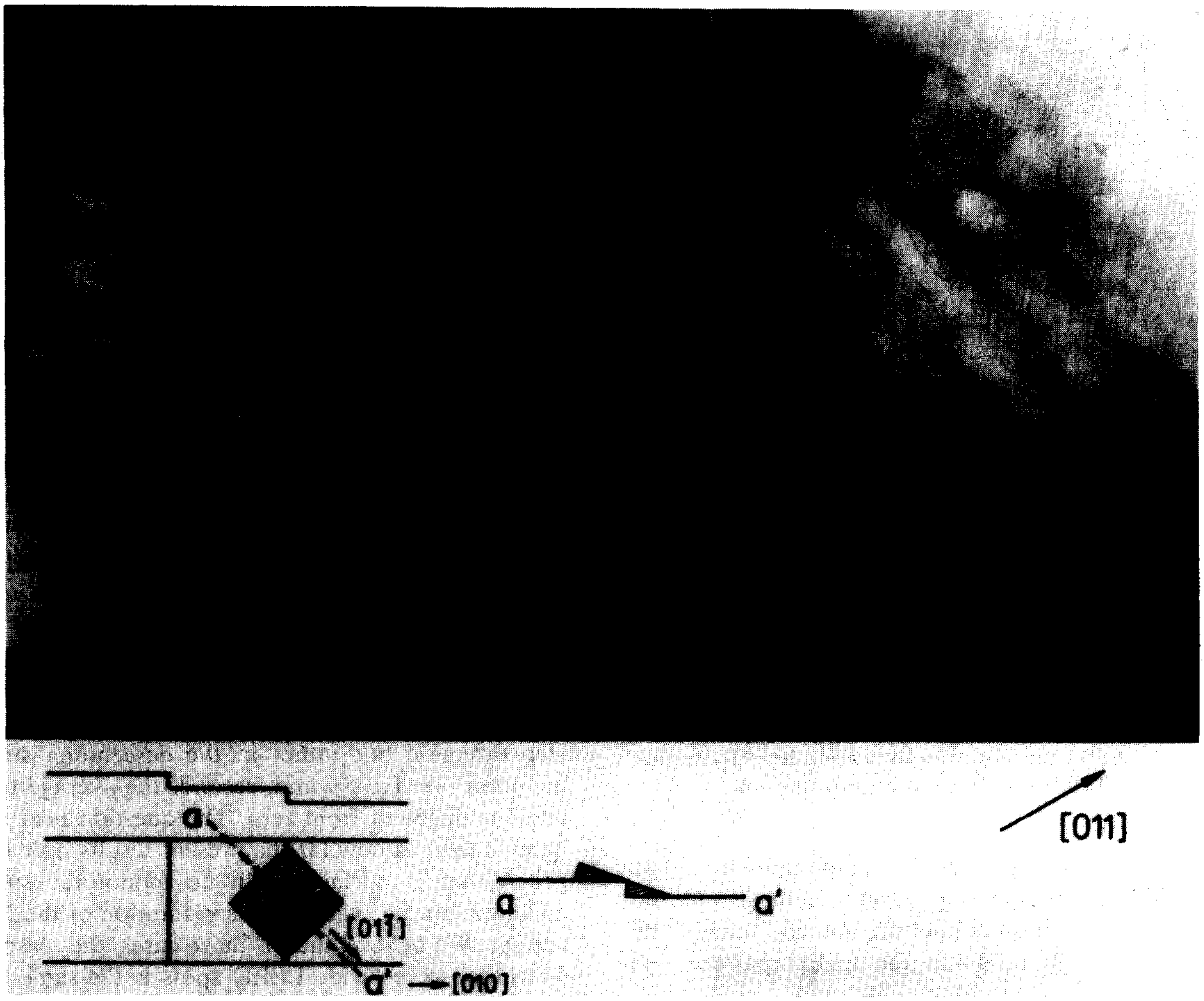

Fig. 10. CCT of Ni(100) exposed at 540 K to 5000 L of oxygen (at a pressure of 10^{-5} mbar) showing NiO islands. For optimum ordering of the NiO overlayer the growth procedure was divided in cycles of 1200 L exposure and subsequent annealing to approximately 670 K for 4 min. The image was obtained at $U = -0.1$ V and $I = 0.5$ nA. The size is 600 × 1000 Å^2. In the left lower part of the figure the orientation of the NiO islands (shown by the hatched area) is schematically plotted.

lation, however, has to be based upon models that have been proposed before in the literature.

Holloway and Hudson in 1974 [15] concluded from the analysis of their Auger data that oxide formation happens in three steps: (i) Dissociative adsorption of oxygen and formation of a p(2 × 2) pattern, and eventually of a c(2 × 2) pattern. (ii) Formation of NiO islands at defects of the surface and lateral growth of the islands until the surface is covered with an oxide film. (iii) Growth of the oxide layer perpendicular to the surface. This model was supported by further experimental results such as RHEED data [16], UPS data [18], and RBS data [17]. Theoretical evaluations [44,45] also came to similar conclusions. Mitchell et al. [16], early on claimed that steps at the surface may play the key role in oxide formation.

In contrast to this picture Brundle [13] concluded that the oxide nucleation was triggered by imperfections in the chemisorbed c(2 × 2)O phase. Although it cannot be excluded that part of the crystallites nucleate at such imperfections, our results indicate that under the conditions we chose for the oxide preparation steps of the metal surface

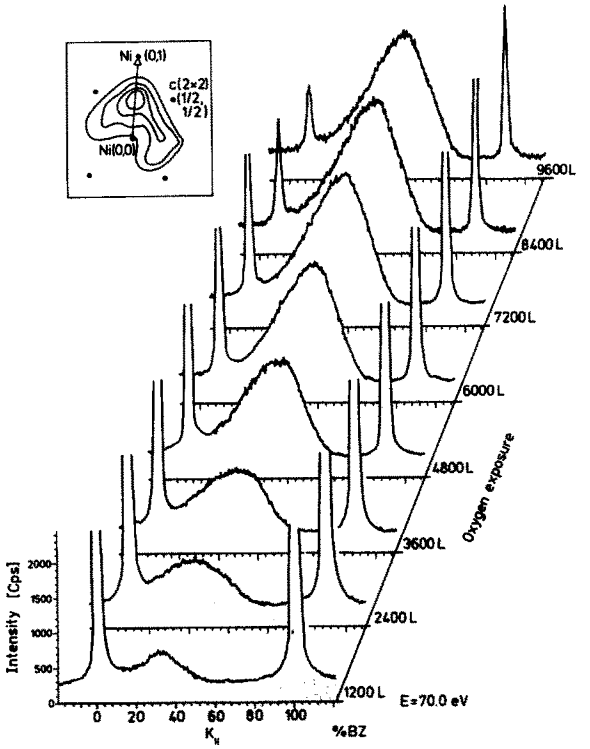

Fig. 11. LEED intensity profiles taken along the [011] direction of Ni(100) for different oxygen exposures.

are the preferred sites for oxide growth. STM shows that on the step edges the most and the largest oxide clusters nucleate and the shift of the NiO(100)-(0,0) reflex in the LEED pattern can only be explained if the crystallites grow at the step edges.

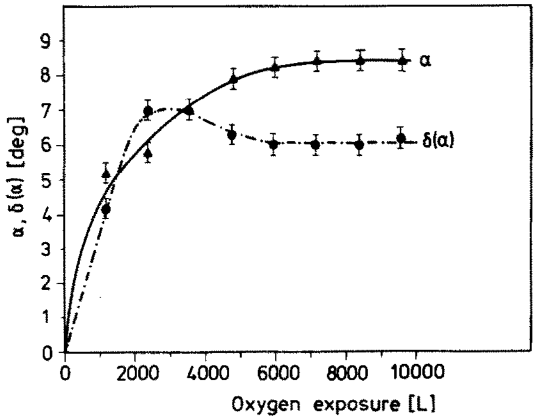

Fig. 12. Tilting angle of the NiO crystallites on Ni(100) and FWHM of the tilting angle distribution as a function of the oxygen exposure.

After nucleation has taken place, NiO islands start to grow. Due to the relatively large misfit between Ni and NiO lattice constants the surface stress on the oxide islands increases in the growing process. The largest part of the stress may be reduced by a tilting of the islands with respect to the metal surface plane. The correlation between tilt direction and step direction may be interpreted in such a way that Ni atoms from the steps migrate underneath the NiO islands and lift the islands. If growing of the islands is particularly fast along the [011]-like directions the surface stress is particularly pronounced in these directions, which in turn explains the preferred tilt in those directions. However, the reason causing the [011]-like directions to be the preferred ones for oxidation is not yet evident, and cannot be given on the basis of the present results.

The proposed mechanism explains why, in the case of a monotonically stepped metal surface, first, the NiO islands are not tilted in ascending step direction but rather in the descending step direction (see fig. 8), and, second, the average tilt angle is different from zero. The question near at hand is then in how far the present results may be generalized to surfaces with no monotonic step arrangement, i.e., with no misorientation of the Ni surface. We believe, that in those cases, the reason for the observed wide LEED spots is the same as in the present case, i.e., a mosaic structure of the NiO film, but that the average tilt angle is close to zero. In this connection it is interesting to refer to unpublished data by Korte and Meyer-Ehmsen [46], who found via RHEED experiments a mosaic structure even on a strongly defect covered (100) surface of a bulk NiO sample. This demonstrates the stability of such a mosaic structure for a thin surface film as well as for a bulk NiO structure.

4. Conclusions

To conclude we would like to come back to the question raised in the introduction about the consequences of the present structural analysis to the adsorption behaviour of molecules on the NiO surface, and to the use of a thin NiO film as a model system for a polycrystalline NiO catalyst with its many different surface defects.

In a previous study [26] it was found that the adsorption of NO on a thin NiO film with a (100) surface mainly takes place on ideal surface sites.

Indirectly these results were supported by the findings of Platero et al. [47] who investigated NO adsorption on polycrystalline NiO of varying perfection. Those samples consisting mainly of NiO crystallites with (100) orientation revealed an NO stretching frequency in perfect agreement with the results on the NiO(100) film. The results of the present study allow us to more closely evaluate the previous findings with respect to the importance of defects on the adsorption behaviour.

The following statements summarize the results relevant with respect to this issue:

(i) The NiO film consists of crystallites which, similar to the situation at the surfaces of a polycrystalline material, provide ideal surface adsorption sites.

(ii) Those regions of the thin film between the crystallites, which cover about 20–25% of the total surface area, must exhibit a large number of different defect adsorption sites.

(iii) The high oxygen content of the NiO film, as suggested by XPS results published earlier [26], points towards the existence of a larger number of Ni^{3+} sites. This type of defect is commonly known, beside the vacancy, to be the most frequently observed point defect in bulk NiO [48].

Therefore, even with these defects present on the surface the adsorption behaviour is dominated by the ideal surface sites [26].

One possible conclusion from (i)–(iii) may be that it is not the structural defect site that induces certain catalytic effects but rather the chemical modification of the surface, i.e., by water etc., that induces catalytically active sites. Studies in these directions shall be carried out in the near future.

Acknowledgements

This work has been supported by the Deutsche Forschungsgemeinschaft (Forschergruppe Modellkat). H.J.F. thanks the Fonds der chemischen Industrie for financial support.

References

[1] A.U. MacRae, Surf. Sci. 1 (1964) 319.
[2] C.R. Brundle and J.Q. Broughton in: The Chemical Physics of Solid Surfaces and Heterogeneous Catalysis, Vol. 3, Eds. D.A. King and D.P. Woodruff (Elsevier, Amsterdam, 1991) to be published.
[3] J.W.M. Frenken, J.F. van der Veen and G. Allan, Phys. Rev. Lett 51 (1983) 1876.
[4] J.W.M. Frenken, R.G. Smeenk and J.F. van der Veen, Surf. Sci. 135 (1983) 147.
[5] P.F.A. Alkemade, S. Deckers, F.H.P.M. Habraken and W.F. van der Weg, Surf. Sci. 189/190 (1987) 161.
[6] U. Starke, P.L. deAndres, D.K. Saldin, K. Heinz and J.B. Pendry, Phys. Rev. B 38 (1988) 12277.
[7] S.Y. Tong and K.H. Lau, Phys. Rev. B 25 (1982) 7382.
[8] J. Stöhr, R. Jaeger and T. Kendelewicz, Phys. Rev. Lett. 49 (1982) 142.
[9] G. Hanke, E. Land, K. Heinz and K. Müller, Surf. Sci. 91 (1980) 551.
[10] N.H. Brongersma and J.B. Theeten, Surf. Sci. 54 (1976) 519.
[11] J.E. Demuth, H.J. DiNardo and G.S. Cargill III, Phys. Rev. Lett. 50 (1983) 1373.
[12] D.E. Taylor and R.L. Park, Surf. Sci 125 (1983) L73.
[13] C.R. Brundle, J. Vac. Sci. Technol. A 3 (1985) 1468.
[14] C.R. Brundle, R.J. Behm and J.A. Barker, J. Vac. Sci. Technol. A 2 (1984) 1038.
[15] P.H. Holloway and J.B. Hudson, Surf. Sci. 43 (1974) 123.
[16] D.F. Mitchell, P.B. Sewell and M. Cohen, Surf. Sci. 61 (1976) 355.
[17] R.G. Smeenk, R.M. Tromp, J.W.M. Frenken and F.W. Saris, Surf. Sci. 112 (1981) 261.
[18] P.R. Norton, R.L. Tapping and J.W. Goodale, Surf. Sci. 65 (1977) 13.
[19] H. Hopster and C.R. Brundle, Le Vide 201 (1981) 285.
[20] F.T. Wagner and T.E. Moylan, J. Electrochem. Soc. 136 (1989) 136.
[21] R.S. Saiki, A.P. Kaduwela, J. Osterwalder, C.S. Fadley and C.R. Brundle, Phys. Rev. B 40 (1989) 1586.
[22] G. Dalmai-Imelik, J.C. Bertolini and J. Rousseau, Surf. Sci. 63 (1977) 67.
[23] J.P.S. Badyal, X. Zhang, R.M. Lambert, Surf. Sci. Lett. 225 (1990) L15.
[24] S.R. Chubb, P.M. Marcus, K. Heinz, K. Müller, Phys. Rev. B 41 (1990) 5417.
[25] W.-D. Wang, N.J. Wu and P.A. Thiel, J. Chem. Phys. 92 (1990) 2025.
[26] H. Kuhlenbeck, G. Odörfer, R. Jaeger, G. Illing, M. Menges, T. Mull, H.-J. Freund, M. Pöhlchen, V. Staemmler, S. Witzel, C. Scharfschwerdt, K. Wennemann, T. Liedtke and M. Neumann, Phys. Rev. B 43 (1991) 1969.

[27] E. Kopatzki and R.J. Behm, to be published.
[28] Th. Berghaus, A. Brodde, H. Neddermeyer and St. Tosch, Surf. Sci. 184 (1987) 273.
[29] R. Franchy, M. Wuttig and H. Ibach, Surf. Sci. 215 (1989) 65.
[30] Th. Berghaus, A. Brodde, H. Neddermeyer and St. Tosch, Surf. Sci. 193 (1988) 235.
[31] M. Henzler, in: Electron Spectroscopy for Surface Analysis, Ed. H. Ibach, Vol. 4 of Topics in Current Physics (Springer, Berlin, 1977).
[32] M.G. Lagally, in: Solid State Physics: Surfaces, Eds. R.L. Park and M.G. Lagally, Vol. 22 of Methods of Experimental Physics (Academic Press, New York, 1985).
[33] M. Henzler, Appl. Phys. A 34 (1984) 205.
[34] M. Henzler, Appl. Surf. Sci. 12/13 (1982) 450.
[35] O. Jusko, P. Marienhoff and M. Henzler, Appl. Surf. Sci. 40 (1990) 295.
[36] D.E. Taylor and R.L. Park, Surf. Sci. 125 (1983) L73.
[37] J.K. Zuo, R.A. Harper and G.C. Wang, Appl. Phys. Lett. 51 (1987) 250.
[38] M. Henzler and M. Marienhoff, J. Vac. Sci. Technol. B 2 (1984) 346.
[39] D.G. Welkie and M.G. Lagally, J. Vac. Sci. Technol. 17 (1980) 453.
[40] H.M. Clearfield, D.G. Welkie, T.M. Lu and M.G. Lagally, J. Vac. Sci. Technol. 19 (1981) 323.
[41] U. Scheithauer, G. Meyer and M. Henzler, Surf. Sci. 178 (1986) 441.
[42] T.S. Rahman, D.L. Mills, J.E. Black, J.M. Szeftel, S. Lehwald and H. Ibach, Phys. Rev. B 30 (1984) 589.
[43] Landolt-Börnstein, Zahlenwertè aus Physik, Chemie, Astrophysik, Geophysik und Technik, Vol. 1, Part 4 (Springer, Berlin, 1955).
[44] S. Reindl, G.M. Pastor and K.H. Bennemann, Surf. Sci. 211/212 (1989) 912.
[45] B. Chakraborty, S. Holloway and J.K. Nørskov, Surf. Sci. 152/153 (1985) 660.
[46] U. Korte and G. Meyer-Ehmsen, to be published.
[47] E. Escalano Platero, S. Coluccia and A. Zecchina, Langmuir 1 (1985) 407.
[48] H. Schmalzried, Solid State Reactions (Verlag Chemie, Weinheim, 1981).